9th International Conference on Fracture Mechanics of Concrete and Concrete Structures
FraMCoS-9
V. Saouma, J. Bolander, and E. Landis (Eds)

DOI 10.21012/FC9.305

RANDOM LATTICE PARTICLE MODELING OF DAMAGE LOCALIZATION IN CONCRETE MEMBERS UNDER COMPRESSION

ALESSANDRO FASCETTI[*], NICOLA NISTICÓ[†] AND JOHN E. BOLANDER[‡]

[*]Sapienza Universitá di Roma
Roma, Italy
e-mail: alessandro.fascetti@uniroma1.it

[†]Sapienza Universitá di Roma
Roma, Italy
e-mail: nicola.nistico@uniroma1.it

[‡]University of California
Davis, CA USA
e-mail: jebolander@ucdavis.edu

Key words: Concrete, Fracture Mechanics, Random Lattice Particle Modeling, Multiscale Experimental Campaign

Abstract. The ability to predict the localization of damage in concrete members subject to uniaxial compression is investigated by means of a recently developed random lattice particle model. Such capability is of great interest in the modeling of concrete structures, since most of the existing models rely on the a-priori definition of a zone in which the nonlinear behavior is concentrated. Lattice particle models, by explicitly representing the mesoscale structure of the material, are capable of simulating the localization of damage. Herein, aggregate particles are represented by poly-sized spheres embedded in a cementitious matrix. The connectivity among particles is defined by a Delaunay tetrahedralization of the sphere centers; the resisting areas of the lattice struts are evaluated by a graph that is dual to the tetrahedralization. The mesoscale mechanical properties used in the simulations were measured as part of a multiscale experimental campaign, which also served to validate the numerical macroscopic response of concrete elements subjected to uniaxial compression.

1 INTRODUCTION

Lattice models are a promising means for simulating damage phenomena in cementitious composite materials. The basic assumption is that the behavior of a three-dimensional body can be modeled by means of uni-dimensional elements (the lattice elements or struts) that interconnect a set of nodal points. Whereas such points can be uniformly or randomly positioned in the domain, randomly generated lattices tend to suffer less mesh-induced bias on cracking direction. A variety of lattice models have been developed and successfully applied to simulating the behavior of concrete materials and structures [1–7].

Being relatively new to the structural engineering field, such models still present open questions. For example, there is a need for determining the mechanical properties to be assigned to the lattice elements. This work proposes a systematic way to evaluate the input properties by means of mesoscale experimental tests. The small specimens are easily and economically produced and tested, making this ap-

proach advantageous and worthy of further investigations.

2 MODEL DEFINITION

The random particle lattice model is composed of a set of nodal sites, which represent the center of the coarse aggregates contained in the concrete [1, 5]. To this end, two considerations arise: 1) the mechanical behavior of the inclusions is directly modeled, enabling mesoscale simulations of the material; and 2) due to computational demand, it is only possible to simulate a coarse fraction of the concrete aggregates. In the present work, a volume fraction of aggregate equal to 35% was obtained.

The generated particles are interconnected by uniaxial elements defined by means of a Delaunay tetrahedralization of the point set. The element stiffness and inertial properties are defined by a modification of the Voronoi tessellation of the same set of points [8].

2.1 Random Placement of Particle Centers

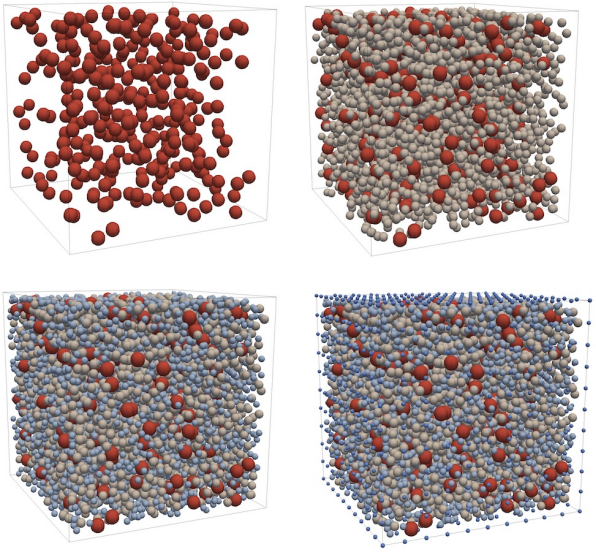

Figure 1: Insertion of particles in the domain for three different granulometric sizes and placement of the external nodes

The number of particles of each granulometric class are calculated as follows:

1. The total volume of aggregate V_a in the sample is prescribed.
2. Based on the given maximum aggregate diameter d_{max} and q exponent of the chosen granulometric curve, it is possible to evaluate the passing amount (%) for every granulometric class chosen (generally chosen equal to the nominal sieve sizes used in practice). Knowing the passing amount for every class, the retained percent is simply calculated as the difference between the adjacent classes' passing.
3. Knowing the retained percent of every class, the total volume of the class is evaluated, and so the number of particles per class.

Having calculated the number of particles per granulometric class, aggregate pieces are inserted in the domain by means of a pseudo-random coordinate generator, guaranteeing no intersection between any of them. Spheres are inserted from biggest to smallest, as shown in Fig. 1.

2.2 Domain Discretization

After the particles have been successfully placed, it is necessary to define the connectivity between their centers. One efficient way to do this is to perform a triangulation (in 2D) or a tetrahedralization (in 3D) of the previously generated set of points.

The Voronoi tessellation of a 3-dimensional domain is widely used in different lattice model approaches. As shown by Bažant et al. [1], however, this choice is not optimal in the case of lattice particle models, since the evaluated contact surfaces tend to intersect the aggregate particles. For this reason, a modified Voronoi tessellation is used, as defined in [8], so that 12 triangles are constructed for each tetrahedron in the mesh (Fig. 2). Such triangles insist on the center of mass of the tetrahedrons, their edges and triangular faces, having calculated these points by only considering the matrix counterparts.

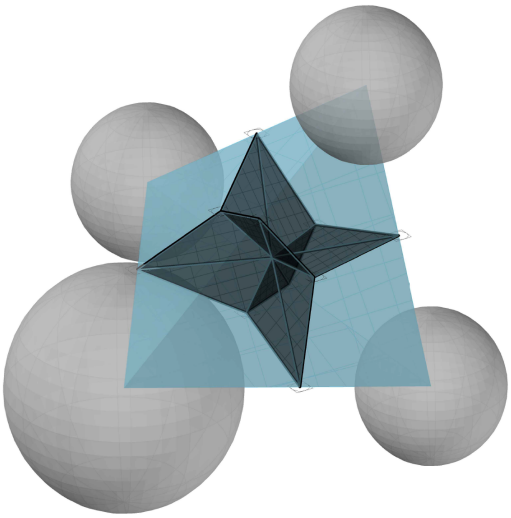

Figure 2: 3-D view of the twelve facets of the modified Voronoi diagram

The so defined tessellation procedure has the following appealing features:

1. it is dual to the Delaunay tetrahedralization; and

2. it only provides contact areas that lie inside the cement paste, which is the location of possible damage.

The collection of all the facets pertaining to the edges emanating from a point represents the point's cell (Fig. 3) and it can be seen as its influence volume. Every particle will share forces with neighbors over the different surfaces of the cell.

Fig. 4 shows two adjacent cells and their contact area. This area is composed of a variable number of triangles, depending on how many tetrahedra contain that particular edge.

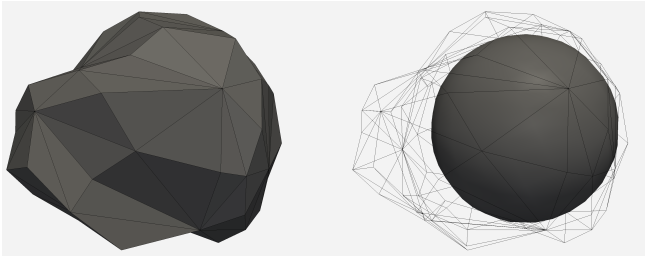

Figure 3: Two different views of one typical cell

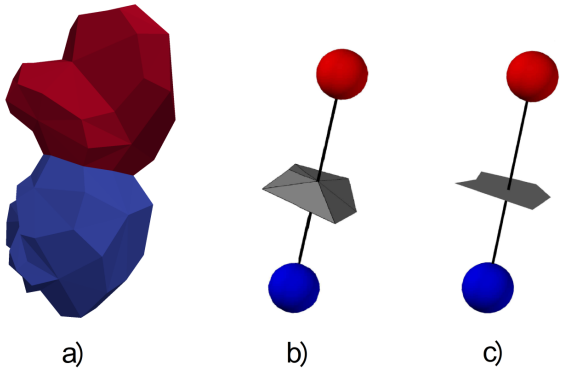

Figure 4: Adjacent cells, the contact area between the cells, and its projection on a plane orthogonal to the element axis

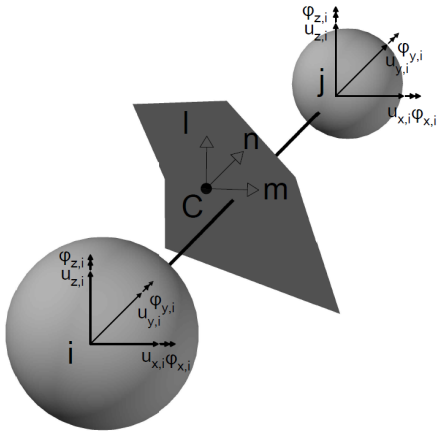

Figure 5: Particle degrees of freedom and connection local axes

The constitutive law is imposed on the projection of such triangles (Fig. 4) on a plane orthogonal to the connection. Such plane is identified by the effective mid-point of the edge G_{ij} and the $\mathbf{n}$ unit vector (see Fig. 5). This choice is due to the asymmetric behavior of concrete in tension and compression. If the constitutive law was imposed on the original facets, in fact, a simple shear in the connection, generated by a relative displacement vector orthogonal to the edge, would also imply tension or compression, leading to different results for the shear response, depending on its direction. This phenomenon is clearly non-physical, therefore the choice of considering the projected contact area is adopted [5].

2.3 Kinematics

Each cell is considered to be rigid, so that the displacement of any point can be calculated as:

$$\mathbf{u}(\mathbf{x}) = \mathbf{u}_i + \theta_i \times (\mathbf{x} - \mathbf{x}_i) = \mathbf{A}_i(\mathbf{x})\mathbf{U}_i \quad (1)$$

where $\mathbf{A}_i$ is:

$$\mathbf{A}_i(\mathbf{x}) = \begin{bmatrix} 1 & 0 & 0 & 0 & z - z_i & y_i - y \\ 0 & 1 & 0 & z_i - z & 0 & x - x_i \\ 0 & 0 & 1 & y - y_i & x_i - x & 0 \end{bmatrix} \quad (2)$$

The vector $\mathbf{U}_i = [\mathbf{u}_i\, \theta_i]^T$ collects the displacement and rotations of node i. By calculating the displacement of point C associated with each adjacent node, i and j, (Fig. 5), the displacement jump at point C can be determined. The strain components are obtained by dividing the displacement jump by the edge length:

$$\epsilon_N = \frac{\mathbf{n}^T[|\mathbf{u}_c|]}{l^e},\ \epsilon_M = \frac{\mathbf{m}^T[|\mathbf{u}_c|]}{l^e},\ \epsilon_L = \frac{\mathbf{l}^T[|\mathbf{u}_c|]}{l^e} \quad (3)$$

where $\mathbf{n}$, $\mathbf{l}$, $\mathbf{m}$ are the local axes of the strut (see Fig. 5). By using this definition it is possible to write:

$$\epsilon = \begin{bmatrix} \epsilon_N \\ \epsilon_L \\ \epsilon_M \end{bmatrix} = \mathbf{B}^{(e)}\mathbf{U}^{(e)} \quad (4)$$

where $\mathbf{U}^{(e)} = [\mathbf{U}_i\mathbf{U}_j]^T$ is the element displacement vector and $\mathbf{B}^{(e)}$ is the compatibility matrix:

$$\mathbf{B}^{(e)} = \frac{1}{l^e}\begin{bmatrix} -\mathbf{n}^T\mathbf{A}_1 & \mathbf{n}^T\mathbf{A}_2 \\ -\mathbf{l}^T\mathbf{A}_1 & \mathbf{l}^T\mathbf{A}_2 \\ -\mathbf{m}^T\mathbf{A}_1 & \mathbf{m}^T\mathbf{A}_2 \end{bmatrix} \quad (5)$$

2.4 Proposed Constitutive Modeling

The constitutive equations should be able to reproduce the material behavior at the finer scale chosen for discretization, so that the numerically evaluated macroscopic response fits the experimental evidence. Herein, the *Elastic Behavior* is defined by:

$$\begin{aligned} \sigma_N &= E_N\epsilon_N \\ \sigma_T &= E_T\epsilon_T = \alpha E_N\epsilon_T \end{aligned} \quad (6)$$

where $\sigma_T = (\sigma_L^2 + \sigma_M^2)^{1/2}$, $\epsilon_T = (\epsilon_L^2 + \epsilon_M^2)^{1/2}$, E_N is the Young's Modulus in the normal direction and α represents the E_T/E_N ratio. As shown by Cusatis et al. [5], the macroscopic elastic behavior of the lattice, in terms of Young's modulus and Poisson's ratio, can be evaluated by means of the following:

$$\begin{aligned} E_0 = \frac{1}{1-2\nu}E \iff E = \frac{2+3\alpha}{4+\alpha}E_0 \\ \alpha = \frac{1-4\nu}{1+\nu} \iff \nu = \frac{1-\alpha}{4+\alpha} \end{aligned} \quad (7)$$

where E_0 is the mesoscale Young's modulus.

The *Fracturing Behavior* is characterized by $\epsilon_N > 0$. Tensile and shear fracture is irreversible, so that the damage controlling parameter must be history-dependent. To this end, the evaluation of damage must be performed on the maximum value of the deformation attained by the element during the load history.

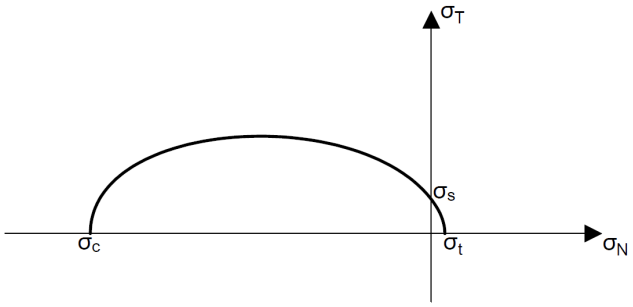

Figure 6: Stress boundary in the $\sigma_N - \sigma_T$ space

The interaction between the normal and tangential behavior of the struts is controlled through a stress boundary, which is defined as an ellipse in the $\sigma_N - \sigma_T$ space (Fig. 6), defined by the σ_t, σ_c and σ_s values:

$$\sigma_N(\sigma_N - \sigma_c - \sigma_t) - \frac{\sigma_c\sigma_t}{\sigma_s^2}\sigma_T^2 = -\sigma_c\sigma_t \quad (8)$$

It is useful to introduce the *effective stress and strain* [5], defined as:

$$\epsilon = \sqrt{\epsilon_N^2 + \alpha\epsilon_T^2},\ \sigma = \sqrt{\sigma_N^2 + \frac{\sigma_T^2}{\alpha}} \quad (9)$$

and the *coupling strain*:

$$tan\,\omega = \frac{\epsilon_N}{\sqrt{\alpha}\epsilon_T} = \frac{\sigma_N\sqrt{\alpha}}{\sigma_T} \tag{10}$$

so that:

$$\begin{cases} \sigma_N & = \sigma\, sin\omega \\ \sigma_T & = \sqrt{\alpha}\,\sigma\, cos\,\omega \end{cases} \tag{11}$$

By substituting the expressions for σ_N and σ_T in the stress boundary (Eq. 8) it is possible to reduce the problem to a 1-D scalar equation in which σ is the only unknown. It follows that

$$\sigma(\omega) = \frac{sin\omega\,(\sigma_c + \sigma_t) + \sqrt{D}}{2(sin^2\omega - cos^2\omega\,\alpha\sigma_c\sigma_t/\sigma_s)} \tag{12}$$

in which

$$\begin{aligned} D \;=\; & sin^2\omega\,(\sigma_c + \sigma_t)^2 \\ & -4\sigma_c\sigma_t(sin^2\omega - cos^2\omega\,\alpha\sigma_c\sigma_t/\sigma_s^2) \end{aligned}$$

Also, ω represents the angle that the stress state line creates with the positive side of the σ_T axis, while $\sigma(\omega)$ the distance from the origin to the stress boundary for that direction. The fracturing mesoscale behavior of concrete exhibits softening for both normal and tangential strain histories. This phenomenon is modeled by imposing that the evolution of the stress boundary follows the exponential rule:

$$\sigma_b(\omega) = \sigma_0\, e^{-\frac{H}{\sigma_0}(<\epsilon_1 - \epsilon_0>)} \tag{13}$$

where ϵ_1 is the maximum value of the deformation previously attained in the connection (history dependent) and ϵ_0 the strain at peak strength.

One of the main advantages in using a lattice approach is the possibility to enforce the correct energy dissipation under basic fracturing modes on the 1-dimensional elements composing the domain. By using scalar relationships between stresses and strain it is possible to scale the constitutive law to impose that every connection dissipates the desired energy during fracture processes. This procedure is needed since damage localizes also at the mesolevel [5].

The fracture energies for pure tension G_t and pure shear G_s are thought to be material properties [1] and therefore their values are constant. Based on this assumption, it is possible to evaluate the H parameter to be used in Eq. 13 to obtain a value of the fracture energy density in the element to satisfy $G_f = l\int_0^\infty \sigma d\epsilon$. After having calculated the values of H for the two basic modes of fracture:

$$\begin{cases} H(\omega = 0) = & H_s = \frac{2\alpha E_0}{(2\alpha E_0 G_S)/(\sigma_s^2 l) - 1} \\ H(\omega = \pi/2) = & H_t = \frac{2E_0}{(2E_0 G_T)/(\sigma_t^2 l) - 1} \end{cases} \tag{14}$$

the transition between pure shear ($\omega = 0$) and pure tension ($\omega = \pi/2$) is supposed to be smooth and governed by the following exponential equation.

$$H(\omega) = H_s + (H_t - H_s)\left(\frac{2\omega}{\pi}\right)^{n_t} \tag{15}$$

The definition of the fracturing behavior is then completed by the loading-unloading rules. When unloading occurs, the element releases stresses elastically (with stiffness equal to E_N) until its value gets to 0. At that point the stress remains null while the deformation diminishes. While reloading, the same elastic modulus is used, and the stress boundary value σ_b defined in Eq. 13 is enforced, so that the stress can never exceed the threshold value obtained at the maximum strain achieved by the strut during the loading history.

The *Frictional Behavior* ($\epsilon_N <= 0$) at the mesoscale must be able to reproduce the attritive effects that lead to an increase in the shear strength and ductility, together with triaxial hardening and pore collapse for volumetric compression. The interaction between the normal and tangential behavior of the struts is supposed to be controlled by the ellipse in the $\sigma_N - \sigma_T$ space defined in Eq. 8.

Compressive stress states ($\epsilon_N < 0$) are highly dependent on the volumetric effects; in order to take this aspect into account, negative normal strain is decomposed in the volumetric (ϵ_N) and deviatoric (ϵ_D) part, with ϵ_V defined as the average of the volumetric deformations

of the triangular facets composing the contact area, weighted on the area of the facets themselves.

The information on the average volumetric deformation acting in the connection is used to define the compressive stress boundary. It is well known that the post-peak compressive behavior is strongly influenced by volumetric effects. To model this phenomenon the stress boundary in compression is dependent on ϵ_v as follows:

$$\sigma_b = \begin{cases} \sigma_c & \text{if} \epsilon_v \geqslant 0 \\ \sigma_c e^{H/\sigma_c(-\epsilon_v - \epsilon_c)} & \text{if} \epsilon_v < 0 \end{cases} \tag{16}$$

Eq. 16 shows that the post-peak compressive behavior must be able to reproduce the hardening response induced by the pore collapse under high volumetric deformations, while a perfectly plastic behavior is assumed in case of positive volumetric deformation.

Also, the hardening modulus H is thought to be dependent on the volumetric and deviatoric deformation acting in the element:

$$H = H_c/(1 + k_2 < r_{dv} - k_1 >) \tag{17}$$

where r_{dv} is the deviatoric to volumetric strain ratio, and k_1,k_2 are material parameters.

The loading-unloading rules in compression follow the same rule used for the cohesive behavior: the element unloads elastically to zero stress, and then σ_N remains null up to zero deformation. The difference with the tension side of the stress-strain response lies in the fact that there is no damage due to compressive actions, meaning that the reloading branch will always merge with the virgin load curve. The description of the frictional behavior of the lattice struts is then completed by defining the shear response under compression. It is supposed to be dependent on the same ellipse in the $\sigma_N - \sigma_T$ plane. The evolution of the boundary is governed by the exponential law:

$$\sigma_b = \sigma_{T,0}\, e^{-\frac{H}{\sigma_{T,0}} < \epsilon_T - \epsilon_{T,0} >} \tag{18}$$

where $\sigma_{T,0} = \sigma(\omega)\, cos\omega\, \sqrt{\alpha}$ (see Eq. 10). The shear post-peak behavior, similarly to the fracturing behavior case already described, is defined by imposing the two values of the softening modulus H:

$$\begin{cases} H(\omega = 0) = & H_s = \frac{2\alpha E_0}{(2\alpha E_0 G_S)/(\sigma_s^2 l) - 1} \\ H(\omega = -\pi/2) = & H_c = 0 \end{cases} \tag{19}$$

so that the shear response varies smoothly from tension to compression. A fictitious perfectly plastic behavior is supposed for the case of pure compression in order to define the following variation rule for the parameter H as a function of ω:

$$H = H_s - H_s \left(\frac{-2\omega}{\pi} \right)^{n_c} \tag{20}$$

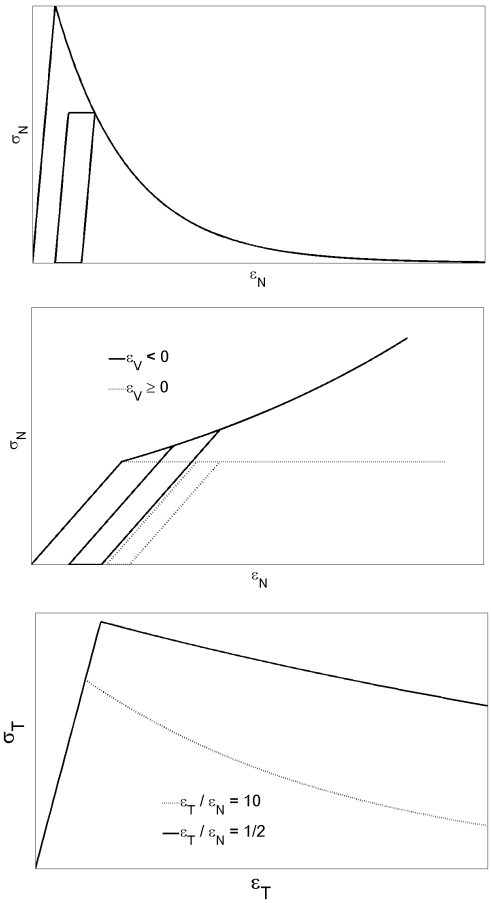

Figure 7: Mesoscale stress-strain response for cyclic tension (top), cyclic compression for different volumetric strain values (middle), shear under different compressive actions (bottom)

3 MULTISCALE EXPERIMENTAL CAMPAIGN

The basic idea behind the laboratory tests is that, by characterizing the mechanical properties of concrete at the mesoscopic scale, it is possible to predict its macroscopic behavior by means of the here proposed lattice particle modeling technique. This approach is particularly advantageous because the dimensions of the specimens can be kept small and the testing procedures can be easily standardized and reproduced without the need of expensive testing systems. Since the materials used were identical for both scales, the goal was to identify the mechanical properties of the mesoscale concrete and use such information in the proposed lattice model, comparing the so obtained macroscopic response.

To this end, a *mesoscale concrete* has been cast in cylindrical elements with the dimensions of the typical struts in the lattice and tested in tension, shear and compression. The so obtained information have been used in the definition of the lattice elements, and the proposed model has been checked against the results obtained on the macroscale lab tests. Such campaign was performed on concrete elements of the usual dimensions used in experiments, cast to have a correspondence with the mesoscale specimens in terms of granulometric composition and materials used.

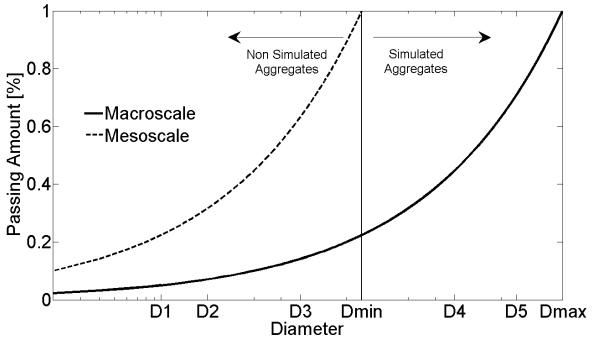

Figure 8: Multiscale granulometric curves used in the experimental tests

3.1 Mesoscale Tests

In most of the simulations conducted in this work, the minimum diameter D_{min} has been set equal to 4.75 mm, which is generally considered as the threshold between the coarse and the fine aggregate. This allows to obtain high inclusion volume fractions while keeping the computational cost reasonable. The mesoscale concrete has so been cast by using aggregate size $D \leq 4.75$ mm (Fig. 8), and it has been tested in shear, tension and compression to evaluate the principal mechanical properties.

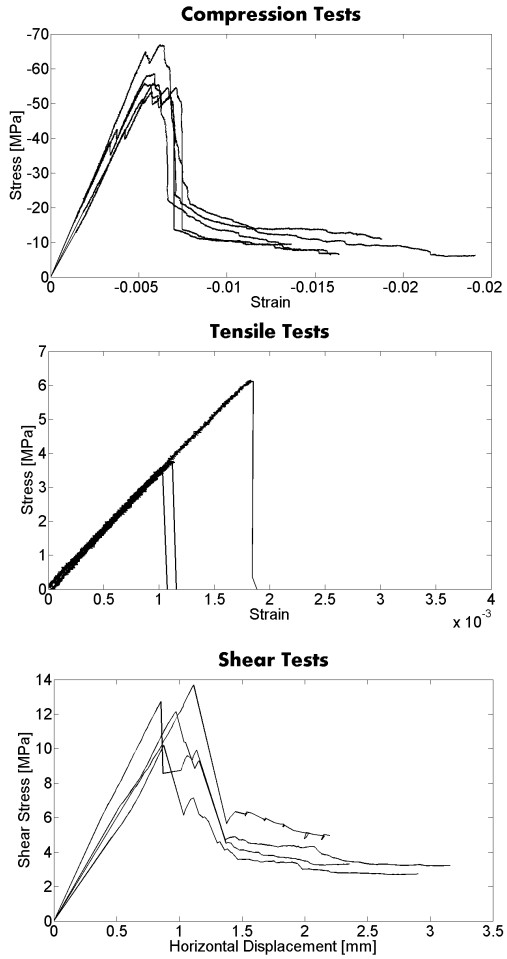

Figure 9: Results of the different tests performed on mesoscale concrete

The first step in the definition of the campaign involved the evaluation of the characteristic dimensions of the mesoscale concrete to be used. Numerical investigations performed on a set of 10 concrete cubes ($l = 150\,mm$) showed

that a diameter equal to 20 mm can be chosen for the mesoscale specimens, since the so obtained value of the cross sectional area is representative of the mean obtained from the model. Cylindrical shape with aspect ratio 2:1 has been used to simplify the test procedure. Different set of tests have been performed. Tensile and compressive uniaxial tests were conducted by means of a hydraulic Universal Testing Machine, while an opportunely modified shear box has been used to evaluate the tangential stress response of the specimens. The results of such investigations are reported in Fig. 9.

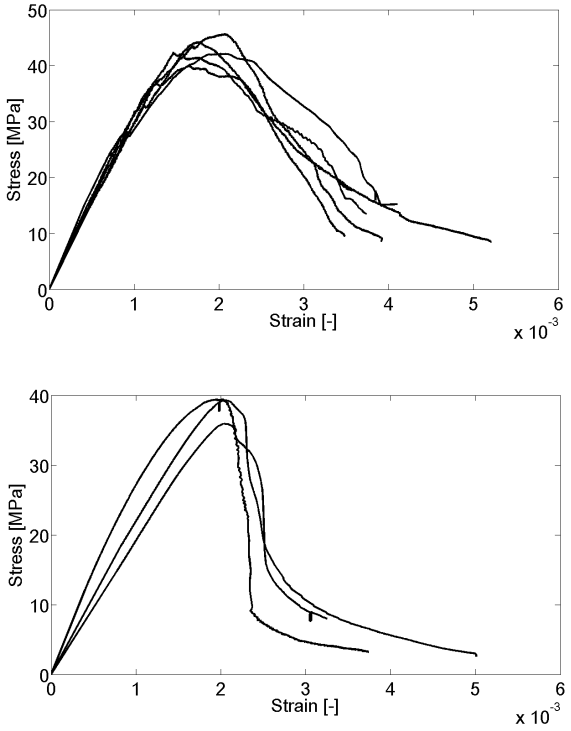

Figure 10: Results of the different tests performed on macroscale concrete: cubical (top) and cylindrical (bottom) specimens

3.2 Macroscale Tests

The mesoscale tests were followed by a *macroscale campaign*, which involved the testing of concrete elements of the usual shape and dimensions (i.e. cylinders, cubes, prisms) used in civil engineering laboratories. A total of six 150 mm cubes and three 300×150 mm cylinders were tested by means of a Universal Testing Machine of capacity 500 kN. Since the materials used were identical for both scales, the goal was to identify the mechanical properties of the mesoscale concrete and use such information in the proposed lattice model, comparing with the so obtained macroscopic response. The experimental results are shown in Fig. 10.

4 NUMERICAL RESULTS

The following sections compare the numerical results with the experimental results from the macroscopic concrete tests.

4.1 Cubic Specimens

The comparison between experimental and numerical responses demonstrates how the model is capable of predicting both the stress-strain curve (Fig. 11) and the crack pattern observed in the tests (Fig. 12). The numerical simulation correctly reproduces the typical ”hourglass” shape of the high friction uniaxial compressive tests, together with a macroscopic shear band that spreads from the top to the bottom of the specimen. Such crack was also observed in the experimental tests, as clearly shown in the figure. A full recap of all the mechanical quantities (i.e. the ones measured in the meso and macroscopic tests, the ones used in the model and those evaluated from the numerical results) is given in Table 1, which shows the correspondence between the mesoscopical values measured in the test, the ones used in the lattice particle model and the macroscopic quantities, both the ones measured in the lab tests and the numerically simulated ones.

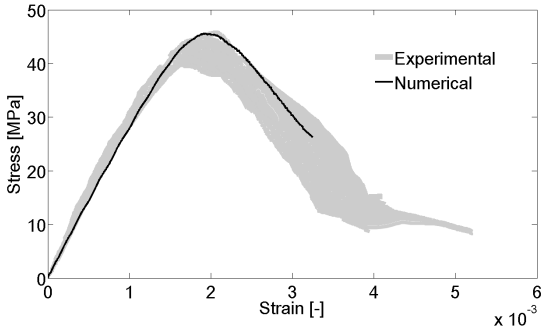

Figure 11: Experimental and numerical stress-strain curves for the cubic specimens

Figure 12: Cubic specimens: experimental and numerical crack pattern at failure

Table 1: Comparison between mesoscopic parameters measured, used and macroscopic quantities measured on the cubic specimens. For the experimentally evaluated quantities, the minimum and maximum measured values are reported.

Quantity	Mesoscale test	Mesoscale input	Macroscale test	Macroscale result
Comp. Strength	52-68 MPa	60 MPa	40-45 MPa	44 MPa
Young's Modulus	42-45 GPa	46.5 GPa	29.8-30.5 GPa	30.1 GPa
Poisson's Ratio	-*	-*	0.178	0.18
Tensile Strength	3.5-6 MPa	4.5 MPa	-	-
Shear Strength	10-13.5 MPa	13.5 MPa	-	-

* Poisson's Ratio was not measured during mesoscale testing. Its value is not a parameter of the model; α is used instead according to Eq. 6.

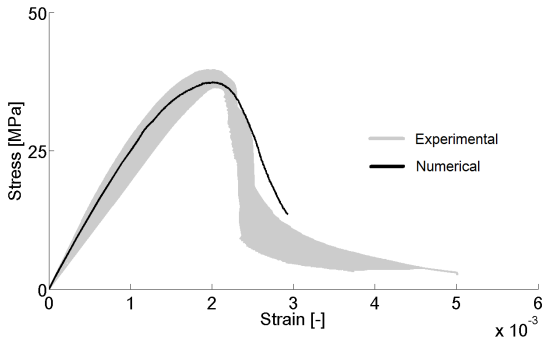

Figure 13: Comparison between experimental and numerical stress-strain curves on cylindrical specimens

4.2 Cylindrical Specimens

The comparison between the experimental and numerical response shows how the model is capable of predicting both the macroscopic stress-strain response (Fig. 13) and the crack pattern at failure. Figure 14 shows how the model is able to localize the damage in a dominant shear band which runs at an angle of approximately $\pi/4$. The direct comparison with the failure mode observed in the experimental tests shows the good agreement with the numerical results. A full recap of all the mechanical quantities used in the model and the corresponding (measured) macroscopic ones is given in Table 2.

Figure 14: Cylindrical specimens: experimental and numerical crack pattern at failure

Table 2: Comparison between mesoscopic parameters measured, used and macroscopic quantities measured on the cylindrical specimens. For the experimentally evaluated quantities, the minimum and maximum measured values are reported

Quantity	Mesoscale test	Mesoscale input	Macroscale test	Macroscale result
Comp. Strength	52-68 MPa	60 MPa	36-41 MPa	37.5 MPa
Young's Modulus	42-45 GPa	46.5 GPa	29.8-30.5 GPa	30.1 GPa
Poisson's Ratio	-*	-*	0.2	0.18
Tensile Strength	3.5-6 MPa	4.5 MPa	-	-
Shear Strength	10-13.5 MPa	13.5 MPa	-	-

* Poisson's Ratio was not measured during mesoscale tests. Its value is not a parameter of the model; α is used instead according to Eq. 6.

5 CONCLUSIONS

A random lattice particle modeling approach to predict fracture phenomena in cementitious materials under compressive actions has been proposed. The numerical results were validated through comparisons with the results obtained on concrete elements tested as a part of a mul-

tiscale experimental campaign. The distinctive features of the presented model are:

1. the discretization of cementitious material is performed by inserting poly-sized spheres in the domain, connecting their centers by means of a Delaunay tetrahedralization and tessellating the domain by means of a modified Voronoi diagram, dual to the tetrahedralization;

2. the stress boundary of the constitutive model is defined as an ellipse in $\sigma_N - \sigma_T$ space, with the advantage of having a continuous law to define such limit. Also, this choice makes it possible to describe both cohesive ($\epsilon_N > 0$) and frictional ($\epsilon_N < 0$) behavior with the same function, simplifying the definition of the material response at the mesoscopic level;

3. the nonlinear post-peak response of the struts shows a smooth transition from pure tension to pure shear to compression, due to the continuity of the relation used to define the softening modulus H as a function of the coupling strain ω.

Herein, mesoscale testing and model calibration were used to successfully predict macroscopic behavior. This presents an attractive, alternative pathway for model validation.

REFERENCES

[1] Bažant Z.P., Tabbara, M.R., Kazemi, M.T., Pijaudier-Cabot, G. 1990. Random particle model for fracture of aggregate or fiber composites. *Journal of Engineering Mechanics* 116(8):1686–1705.

[2] Schlangen, E., van Mier, J.G.M. 1992. Experimental and numerical analysis of micromechanisms of fracture of cement-based composites. *Cement and Concrete Composites* 14: 105–118.

[3] Schlangen, E., Garboczi, E.J. 1997. Fracture simulations of concrete using lattice models: Computational aspects. *Engineering Fracture Mechanics* 57:319-332.

[4] Bolander, J.E., Saito, S. 1998. Fracture analyses using spring networks with random geometry. *Engineering Fracture Mechanics* 61(5): 569-591.

[5] Cusatis, G., Pelessone, D., Mencarelli, A. 2011. Lattice Discrete Particle Model (LDPM) for failure behavior of concrete. I: Theory. *Cement and Concrete Composites* 33(9): 881-890.

[6] Alnaggar, M., Cusatis, G., Di Luzio, G. 2013. Lattice discrete particle modeling (LDPM) of alkali silica reaction (ASR) deterioration of concrete structures. *Cement and Concrete Composites* 41: 45-59.

[7] Fascetti, A. 2016. Random Lattice Particle Modeling of Fracture Processes in Cementitious Materials. PhD Dissertation, Sapienza Universitá di Roma, 170 pp.

[8] Cusatis, G., Bažant, Z.P., Cedolin, L. 2006. "Confinement-shear lattice CSL model for fracture propagation in concrete. *Computer Methods in Applied Mechanics and Engineering* 195(52): 7154-7171.